IRANIAN JOURNAL OF CATALYSIS

Transition-metal modified mesoporous silica nanoparticles as highly effective heterogeneous catalysts for discoloration of Basic red 5 in aqueous solution

Fatemeh Mahfoozi[a], Ali Mahmoudi[a,*], Mohammad Reza Sazegar[a,*], Khodadad Nazari[b]

a) Faculty of Chemistry, North Tehran Branch, Islamic Azad University, Hakimiyeh, Tehran, Iran.
b) Future Bioenergy Solutions Inc., North Vancouver, BC, V7P 3P9, Canada

Received 15 January 2022; received in revised form 21 May 2022; accepted 5 June 2022 (DOI: 10.30495/IJC.2022.1949927.1911)

ABSTRACT

Mesoporous silica nanoparticles (MSNs) were synthesized hydrothermally and modified with Co^{2+} and Zn^{2+}. The as-prepared samples were denoted as MSN, Co-MSN(X), and Zn-MSN(X), where X is the Si/M molar ratio. In addition, co-modified MSN samples with both cations were also prepared and denoted as Co-Zn(Y)-MSN(X), where Y indicates the Zn^{2+} content in the range of 1-7 *wt*.% relative to Co^{2+}. Correctness of the anticipated structures was approved by FTIR, XRD, SEM, EDX, BET, and XRF analyses. It was found that Co-Zn(7)-MSN(75) can be used as an efficient photocatalyst for discoloration of basic red 5 under very mild conditions. Up to 86% of basic red 5 was discolored after 3.75 h under the optimized conditions including catalyst dosage of 0.025 mg mL^{-1}, pH=7, and irradiation of 4×8 W UV (254 nm) lamps. By using the Langmuir–Hinshelwood kinetics model, it was found that the reaction followed a pseudo-first-order kinetic.

***Keywords**: MSN; Photocatalytic; Discoloration; Basic red 5; Modification.*

1. Introduction

Basic red 5 which has also been known as toluylene red, neutral red, or C.I. 50040, is a phenazine dye and has been widely used in nuclear counterstaining in biological research. Loss of cell viability results in loss of basic red 5 uptakes [1]. It has been also used for staining cell cultures in plate titration of viruses, and as an intracellular pH indicator. The toxic nature of the dye can be easily understood by considering its materials safety data sheet (MSDS). Its adverse effects may include carcinogenicity and chronic toxicity. It is noteworthy that about 15% of the total dyes produced worldwide are released during the dyeing processes as effluents [2]. The discharged effluents of dyeing processes pose a potential threat to aquatic organisms, which are the main source of food for many living species. Most of the dyes are highly soluble in water and their removal from water resources is associated with many experimental challenges. Various methods have been devised for the removal of dyes, especially basic red 5. These may include but are not limited to, adsorption, coagulation, photo-catalytic degradation, membrane processes, and advanced oxidation processes (AOPs)[3-8]. These methods however have their drawbacks. For example, adsorption processes are non-destructive and transfer the pollutants from water to another phase, which may cause secondary issues. The other limitations may include the need for special apparatus, costly and complicated work-up, harsh reaction conditions, and so on.

Ordered mesoporous silica nanoparticles (MSNs) were first synthesized using surfactant templates in the early 1990s [9, 10]. Since then, various MSNs have been developed owing to the diversity of surfactants and deep understanding of sol-gel chemistry. Nowadays, MSNs have found their position as stable and tunable scaffolds in catalysis, adsorption, drug delivery, and sensing [11-16]. The size, morphology, and pore structure of mesoporous silica nanoparticles can be finely tuned. With the cetyltrimethylammonium bromide (CTAB) as a structure-directing agent and tetraethyl orthosilicate (TEOS) as the silica source, MCM-41 was firstly synthesized with an array of two-dimensional hexagonal channels [9]. Modification of MSNs has widely been investigated. Surface modification of the MSNs using

*Corresponding author:
E-mail address: *mahmoudiali.ac@gmail.com* (**A. Mahmoudi**) *m_r_sazegar@yahoo.com* (**M. R. Sazegar**)

the abundant surface silanol groups is relatively easy. In addition, the modification of the mesoporous silica nanostructures with transition metals can considerably extend their range of applications [17-22]. In comparison with other porous materials such as activated carbon, MOFs, MWCNTs and mesoporous silica nanoparticles have high thermal stabilities. This is of great importance, when regeneration of the adsorbent, for example via incineration, is considered. On the other hand, physicochemical processes such as photo-degradation methods based on modified MSNs are actively pursued by researchers for wastewater treatment. The course of a photocatalytic degradation involves a series of steps including photon harvesting, production and separation of e/h pairs, their conveyance to the photo-catalyst surface, and finally, generation of radical species such as superoxide and hydroxyl radical, which are responsible for the oxidation of organic molecules to complete mineralization. An important parameter in a photocatalytic process is the e/h recombination. A fast e/h recombination may act as a serious drawback as discussed by Nezamzadeh-Ejhieh et al [23, 24]. To diminish this drawback, various methods have been devised including size reduction, doping, coupling, and supporting on a suitable substrate, as discussed by Rezaei et al, and references therein [23]. In continuation of our research interest in the synthesis and application of modified MSNs, herein, we report the hydrothermal synthesis of mesoporous silica nanoparticles co-modified with Co2+ and Zn2+ and their application as efficient photocatalysts for discoloration of basic red 5 under UV irradiation. A novel aspect of our findings could be that co-modification of the MSNs with transition metals can improve the e/h formation and diminish its recombination, as discussed in the text.

2. Experimental

2.1. Materials

All of the chemicals including tetraethylorthosilicate (TEOS, as the silica source for preparation of MSNs), cetyltrimethylammonium bromide (CTAB, as a template and structure-directing agent), $Co(NO_3)_2.6H_2O$, $Zn(NO_3)_2.6H_2O$, ammonia solution (25%), and basic red 5, were purchased from Sigma-Aldrich and used as received. Double distilled water was used in all of the experiments.

2.2. Methods

X-ray diffraction (XRD) patterns were recorded on a PW 1730 Philips X-ray diffractometer at a scan rate of 0.1º 2θ/s, using Cu-Kα radiation (1.5406 Å). Cobalt content was determined by X-ray fluorescence spectrometry (XRF) utilizing a Bruker S4 Explorer instrument equipped with a rhodium anode at 50 kV and 30 mA. Nitrogen adsorption/desorption measurements were performed at 77 K on a BELSORP-MINI II instrument. Samples were degassed *in vacuo* and annealed at 250 °C for at least 6 h to remove moisture. Barrett–Joyner–Halenda (BJH) model was used for the evaluation of the pore size distribution. The morphology and particle size of the samples were determined by using a scanning electron microscope (SEM KYKY-EM-3200) with an accelerating voltage of 26 kV. Fourier-transform infrared (FT-IR) spectra were recorded on a Rayleigh WQF-510 spectrophotometer using KBr disks. UV-Vis spectra of the dye solutions were recorded on a Varian Cary 100 spectrophotometer using quartz cuvettes.

2.3. Synthesis of mesoporous silica nanoparticles (MSNs)

A previously reported procedure was used for the preparation of the mesoporous silica nanoparticles [21,25]. In a round-bottomed flask, 3.7 g of CTAB was dissolved in 150 mL of double distilled water at 298 K. Then 230 mL of absolute ethanol and 14 mL of 25% ammonia were added, and stirred for 1 h. Afterward, 15 mL of TEOS was added, and the mixture was stirred for 10 h. The white precipitate was aged for 24 h, and then filtered and washed with 50 mL of a mixture of methanol and double distilled water (1:5). The product was dried at 383 K overnight and then calcined at 823 K for 5 h to eliminate the remained organic residues.

2.4. Synthesis of M-MSN (75)

The same experimental procedure as described in 2.3 was used to prepare metal-incorporated MSNs. Before the addition of TEOS, however, 0.9 mmol of either Zn(NO3)2.6H2O (0.265 g), or Co(NO3)2.6H2O (0.262 g) was added to obtain a Si/M ratio of 75 in the final product. The products were denoted as Co-MSN (75) and Zn-MSN (75). I have explained more before [21, 25].

2.5 Synthesis of Co-Zn(X)-MSN (75)

Following previous papers, metal incorporation of MSN was applied [25]. Before the addition of TEOS, appropriate amounts of $Co(NO_3)_2.6H_2O$ and $Zn(NO_3)_2.6H_2O$ were added to the reaction mixture, so that the weight percent of Zn to Co in the final product was 1-7%. For example, in a round-bottomed flask, 3.7 g of CTAB was dissolved in 150 mL of double distilled water at 298 K. Then, 230 mL of absolute ethanol and

14 mL of 25% ammonia were added, and stirred for 1 h. Then 0.262 g of cobalt nitrate hexahydrate and 2.65 mg of zinc nitrate hexahydrate were added to the solution. Afterward, 15 mL of TEOS was added, and the mixture was stirred for 10 h. The white precipitate was kept for 24 h, and then filtered and washed with 50 mL of a mixture of methanol and double distilled water (1:5). The product was dried at 383 K overnight and then calcined at 823 K for 5 h to eliminate the remained organic residues. This product was denoted as Co-Zn(1)-MSN(75). The other products were denoted as Co-Zn(X)-MSN(75), where X is the weight percent of Zn to Co, corresponding to the addition of 2.65, 5.3, 7.95, 10.6, 13.25, 15.9, and 18.55 mg of the $Zn(NO_3)_2.6H_2O$ to the solution.

2.6. Catalytic activity tests

To evaluate the catalytic performance of the modified MSN samples, basic red 5 was selected as a representative toxic dye, and a comparative study was conducted for its discoloration at room temperature with H_2O_2 as an affordable oxidant. To do so, the stock solutions of the catalysts were prepared as follows: 1.5 mg of each catalyst was dispersed in 1.0 mL of sodium acetate-acetic acid buffer solution (pH 4.0, 7.0), or sodium phosphate buffer solution (pH=9.0), by sonication for 15 min. In a typical experiment, 120 µL of 2 mM basic red 5 in acetate buffer, 50 µL of the catalyst stock solution (1.5 mg/mL), and 30 µL of H_2O_2 (0.1 mM) were added into 2800 µL of acetate buffer (pH 4.0, 7.0), or sodium phosphate buffer (pH 9). The trend of discoloration of basic red 5 was studied by UV-Vis spectroscopy after the removal of solids by centrifugation at 5000 rpm. Absorbance changes were measured at λ_{max} of 520 nm with a molar absorptivity of 3.6×10^4 $M^{-1}cm^{-1}$ [26]. A box photoreactor fitted with an array of four UV lamps (8 W, Siemens, Germany, two located at the top, one at the right, and one at the left side of the box) was used in this study. The inner walls were covered with aluminum foil to maximize the irradiated light.

To study the role of environmental matrices, photocatalytic discoloration of basic red 5 was also performed with Tehran's Jajrood river water used instead of double-distilled water, for the preparation of solutions.

3. Results and Discussion

3.1. Characterization of the catalysts

FT-IR spectroscopy was used to evaluate the correctness of the synthesized structures. In **Fig. 1**, the FT-IR spectrum of MSN is compared with its metal-modified forms. Characteristic peaks of the adsorbed water molecules and surface silanol groups appeared at about 3430 cm^{-1} (O-H stretching), and 1620 cm^{-1} (H-O-H, Si-O-H bending), respectively. Symmetric and asymmetric stretching vibrations of the Si-O-Si scaffolds were observed at about 1090 and 800 cm^{-1}, and their corresponding bending vibrations appeared at 460 cm^{-1}. These observations are in agreement with the previously reported results [24, 27]. Although the Co-O and Zn-O vibrations corresponding to the metallic ions in the tetrahedral and octahedral holes are clearly visible in the pure metal oxide spectra, due to their low concentration and similarity of their atomic weights to Si, these were not clearly visible in the FTIR spectra of the modified samples. Hence, modification with either Co^{2+} or Zn^{2+} did not change the intensity and position of the bands significantly. This indicates that the framework structure of the MSN was preserved after metal modification. The simultaneous presence of Co^{2+} and Zn^{2+} also had no considerable effect on the intensity and position of the bands.

The low angle XRD patterns for the pure MSN and its metal-modified forms are presented in **Fig. 2a**. All of the samples showed a strong diffraction peak at about 2.6° corresponding to the (100) plane of the unit cell, along with three weak reflections at 4.3°, 4.75°, and 5.6° indexed to (110), (200), and (210) planes of two-dimensional hexagonal (p6mm) structure of mesoporous silica materials with a d_{100}-spacing of approximately 3.65 nm (JCPDS No. 00-049-1712). One can note that the inclusion of metals has led to a slight shift of the most intense reflection to lower 2θ. The observed shift may be related to the ionic radius. Since Zn^{2+} has a higher ionic radius than Co^{2+}, it increases the d_{100}-spacing more when it replaces silica. It has been suggested that the formation of M-O-Si bonds is responsible for the observed shift in the peak positions [31]. High angle patterns for the synthesized samples are presented in **Fg. 2b.** All of the samples are common in a broad peak around 22° which originates from amorphous silica. These findings are in agreement with the previously published XRD data for the MSN and its modified forms [18, 19, 22]. The average crystallite size of the particles was estimated by both Debye-Scherrer (D=0.9λ/β cos θ) and Williamson-Hall (W-H plot) equations. Both methods resulted in the average crystallite sizes in the range of 20-30 nm, which are in agreement with the SEM imaging results.

In **Fig.** 3, the SEM images of MSN and its metal-modified products are combined with the EXD analysis results. As it is clear, all of the samples appeared as uniform spherical particles with an average size of 100-200 nm.

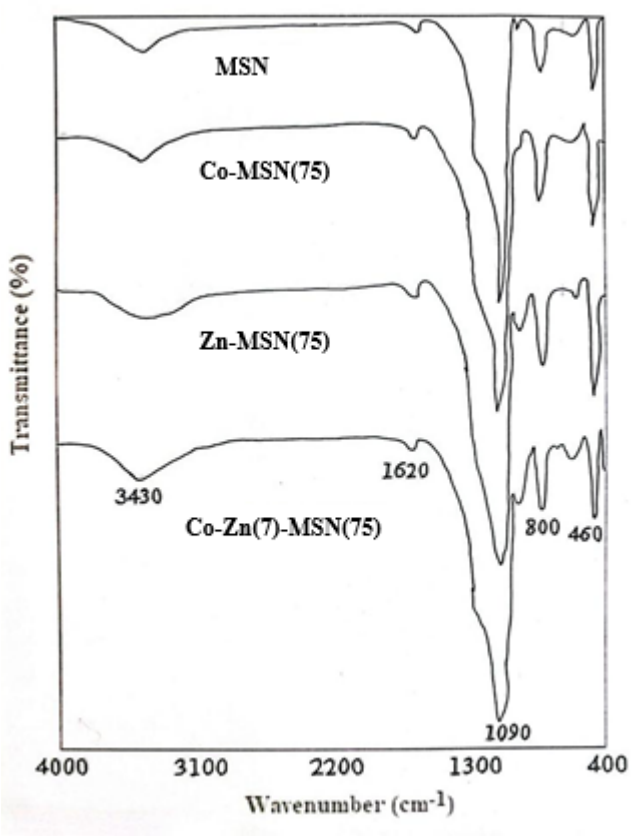

Fig. 1. FT-IR spectra of the MSN and its metal-modified products.

Nevertheless, their rough surfaces appear to consist of smaller nanoparticles ranging from 20-30 nm. It seems that these nanoparticles tend to aggregate to form the larger spherical particles. One can also note that the surface of Zn-MSN(75) and Co-Zn(7)-MSN(75) samples are rougher. This may be due to the higher ionic radius of Zn^{2+}. The existence of Co and Zn was approved by EDX analysis, and as shown in **Fig. 3**, in addition to the strong signals of the Si, C, and O elements, the characteristic K and L lines of the Co and Zn appeared at the anticipated positions. It should be mentioned that the presence of C is related to the method of sample preparation for EDX analysis.

To determine the metal content of the modified MSN samples more accurately, XRF spectroscopy was used. The results are included in Table 1 and indicate that the real Co and Zn contents (1.63, 0.115 *wt.*%) are very similar to those measured by the EDX analysis (1.63, 0.12 *wt.*%).

The data in **Table 1** show that the high surface area of MSN was reduced to some extent after modification with Co^{2+}, and even more, the reduction was observed after modification with Zn^{2+}. As justified in the discussion of d_{100}-spacing, this observation can be related to the higher ionic radius of Zn^{2+}. The reduction in S_{BET} was, even more, when both Co^{2+} and Zn^{2+} were used. A decrease in the S_{BET} can be attributed to the partial blockage of the porous channels, according to Hajiagha et al [21]. The monolayer adsorbed volume (V_m) also showed the same behavior. Thus, the observed trend in the average pore radius is also justifiable.

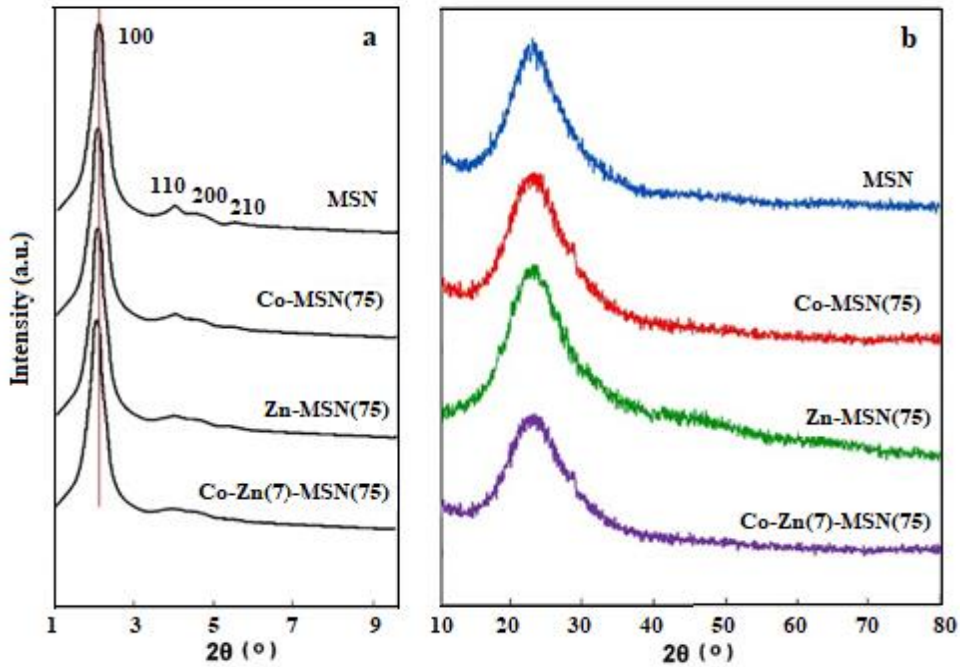

Fig. 2 Low angle (a) and high angle (b) XRD patterns for the MSN and its metal-modified forms.

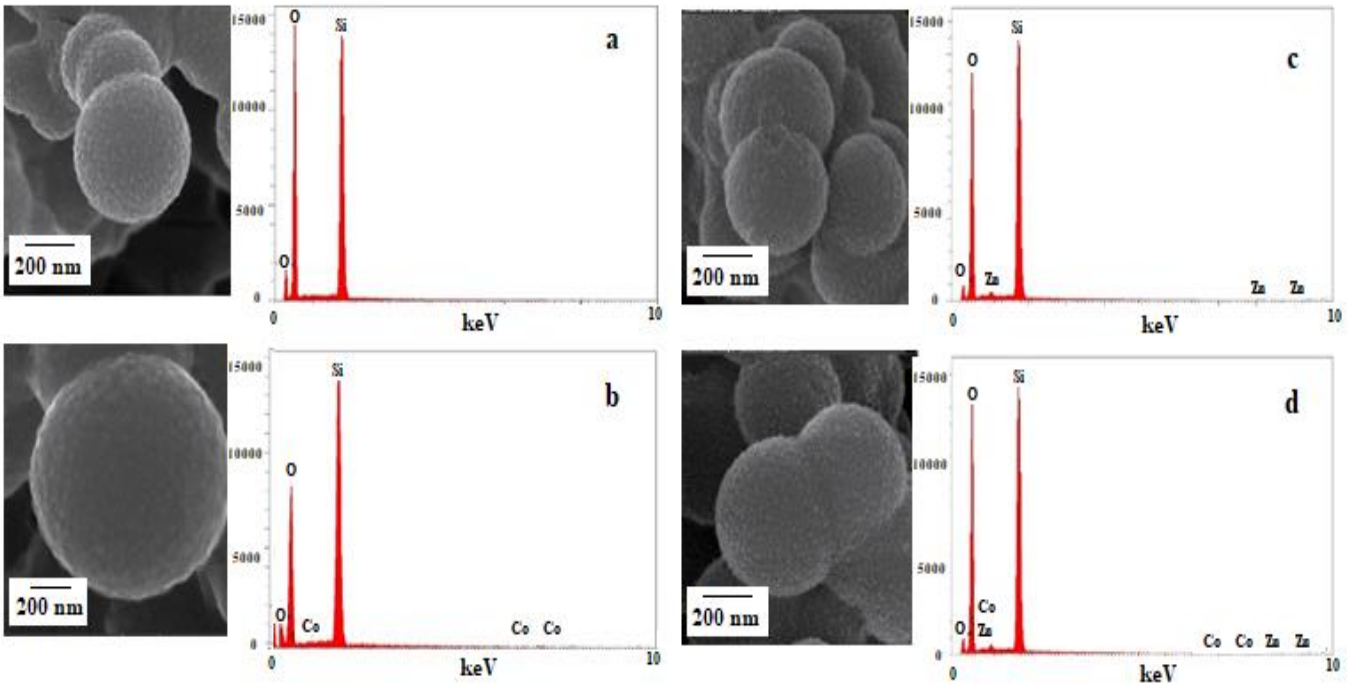

Fig. 3 SEM (left) and EDX analysis (right) of the MSN (a), Co-MSN(75) (b), Zn-MSN(75) (c), and Co-Zn(7)-MSN(75) (d).

Table 1. Physicochemical properties of the synthesized samples

Catalyst	Co^{2+}, Zn^{2+} *wt.%* (Theoretical)	Co^{2+}, Zn^{2+} *wt.%* (XRF)	Co^{2+}, Zn^{2+} *wt.%* (EDX)	S_{BET} [a] (m^2g^{-1})	Average pore radius (nm)	V_m [b] (cm^3g^{-1})
MSN	0.0, 0.0	0.0, 0.0	0.0, 0.0	1062.2	1.34	244.1
Co-MSN(75)	1.63, 0.0	1.625, 0.0	1.63, 0.0	691.5	1.29	158.8
Co-Zn(7)-MSN(75)	1.63, 0.114	1.632, 0.115	1.63, 0.12	602.1	1.21	138.3
Zn-MSN(75)	0.0, 1.81	0.0, 1.80	0.0, 1.82	660.4	1.29	151.7

[a] BET surface area obtained from N_2 adsorption-desorption isotherms; [b] Adsorbed volume.

The N_2 adsorption-desorption isotherms of the MSN and its metal-modified forms are presented in **Fig. 4.** All of the samples represented a type IV isotherm with distinct H4 hysteresis loops in the p/p_0 range of 0.3-1.0, corresponding to well-ordered mesoporous materials. It can be concluded that although the specific surface area of the MSN decreases after metal modification, its mesoporous structure is largely preserved. Sharp inflections of capillary condensation within uniform pores at low relative pressure are indicative of the presence of small pores and volumes [28]. It is also clear that at the higher relative pressure (p/p_0 range of 0.8–1.0), no further enhancement of the adsorbed nitrogen was observed. This may be related to the incorporation of the metal ions into the MSN framework [17]. **Fig. 4** also depicts the BJH plots of dV_p/dr_p versus r_p. One can note that the pore radius is decreased after metal modification, which can be attributed to the higher size of the M^{2+} ions than Si^{4+}.

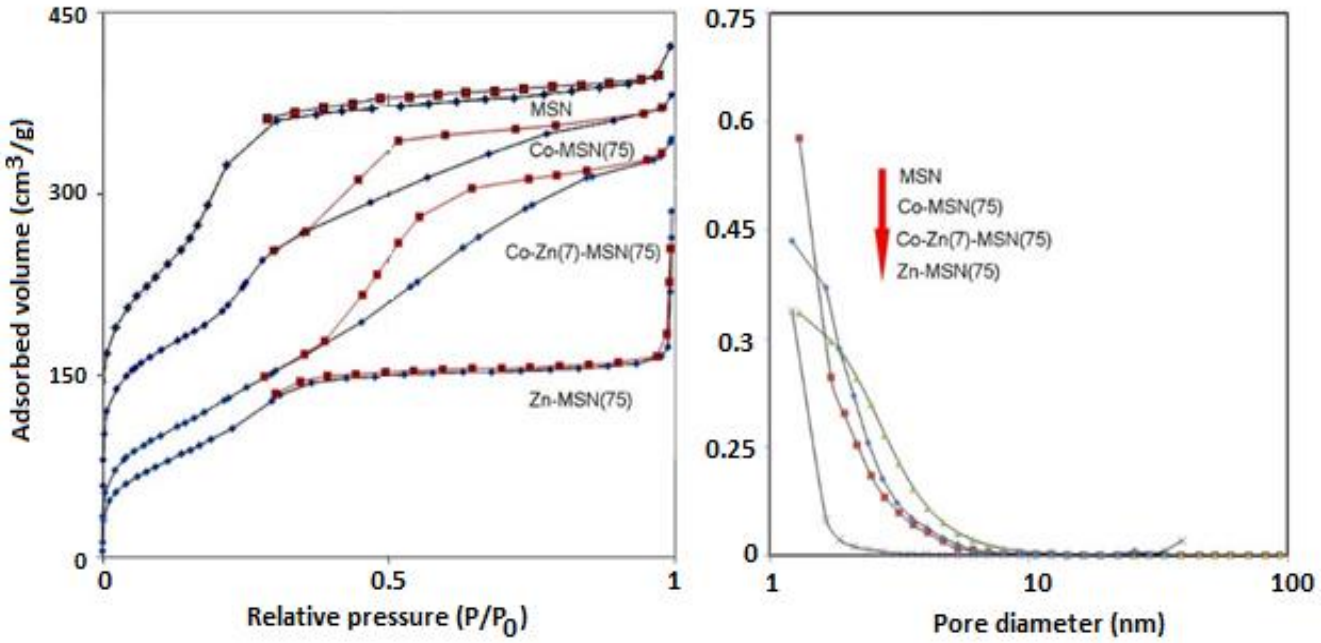

Fig. 4 N_2 adsorption-desorption isotherms of the MSN and its metal-modified forms (left), and corresponding BJH plots (right).

3.2. Photocatalytic degradation of Basic red 5

After characterization of the catalysts, a systematic study was performed to determine the optimum conditions for the degradation of basic red 5. In this regard, the effect of various parameters such as catalyst dosage, metal content, oxidant, UV irradiation, pH, dye concentration, etc. was studied. While pure MSN was not an effective catalyst for the discoloration of basic red 5, it was found that incorporation of Co^{2+} has a meaningful effect on the desired reaction. In **Fig. 5** the trend of discoloration of basic red 5 is plotted as ln C/C_0 versus time in presence of MSN and its Co^{2+}-modified forms. It is clear that the discoloration efficiency depends on the cobalt content. The role of cobalt in the enhancement of the photocatalytic activity of the MSNs can be attributed to its ability to increase photon harvesting and production of e/h pairs. This seems to be related to the cobalt content to some extent. Co-MSN(10) with the Si/Co molar ratio of 10, however, was not as effective as Co-MSN(75), because higher cobalt contents may result in some pore blockage and framework destruction due to the formation of Co_3O_4 nanoparticles [21]. According to the BET analysis data, the cobalt species were well dispersed in the MSN framework, so the metal active sites are more accessible to the substrate. The lowest activity of CoMSN(10) may be related to the generation of the cobalt networking, in addition, a decrease in the surface area is due to the blockage of the pores by cobalt species. It was also found that UV irradiation has a positive effect on discoloration efficiency. Increasing the irradiation power from 16 to 32 W increased efficiency, but no further improvement was observed in higher irradiation power. According to these results, the Co-MSN(75) was used as a basis for further modifications.

It has also been known that Zn^{2+} is an excellent dopant for photocatalytic activity [29]. To study the effect of Zn^{2+} on the activity of MSNs, Zn-MSN(75) with the Si/Zn ratio of 75 was also tested in the desired reaction (**Fig. 6**). It is clear that the efficiency, even in presence of UV irradiation, is not as high as the Co-MSN(75).

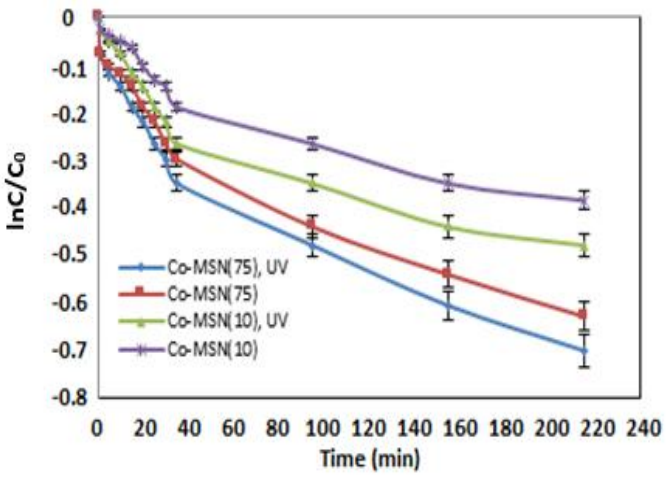

Fig. 5 Trend of degradation of basic red 5 (0.08 mM) in terms of ln C/C_0 in presence of Co^{2+}-modified MSNs with different Si/Co ratios of 75 and 10, with and without UV irradiation at 298 K and pH=7.

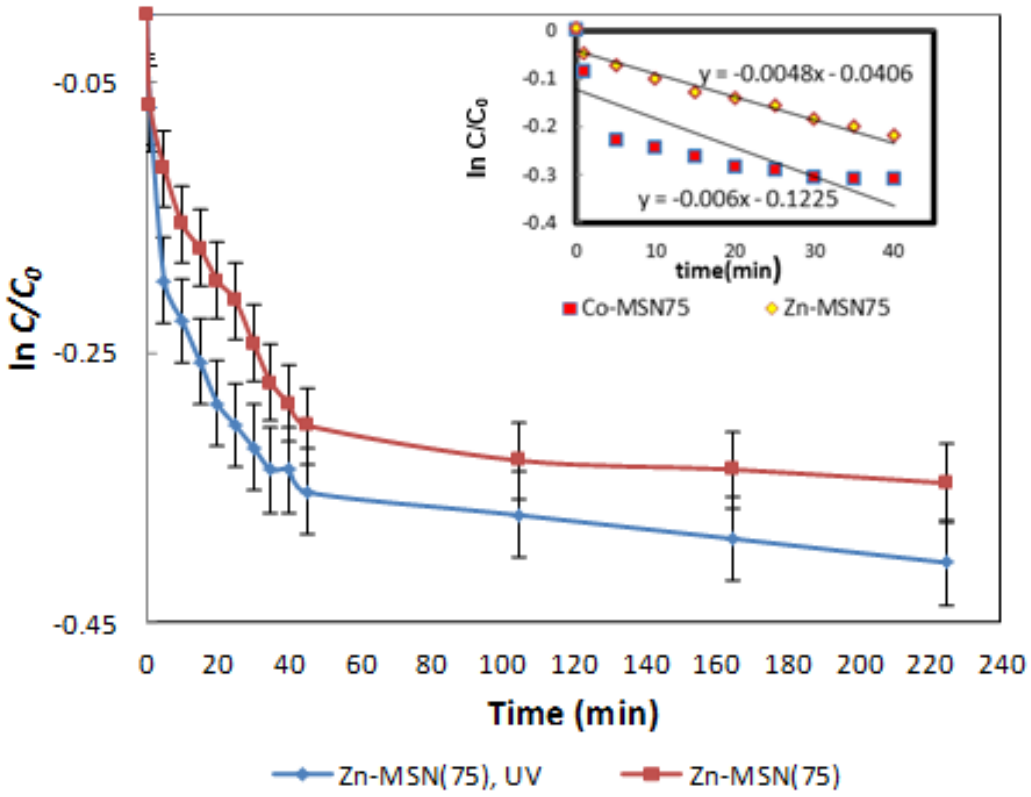

Fig. 6 Trend of degradation of basic red 5 (0.08 mM) in presence of Zn-MSN(75) (0.025 mg) with and without UV irradiation at 298 K and pH 7. The inset of the figure was used for comparison of Co-MSN(75), and Zn-MSN(75).

To justify the role of Zn(II) in the promotion of the photocatalytic discoloration, it can be pointed out that when a photon with energy higher or equal to the bandgap is irradiated to the Zn doped MSNs surface, a photoexcited valence band electron is promoted to the conduction band, leaving behind a hole in the valence band, thus creating e/h pairs. Clearly, doping of Zn in MSN results in a lower bandgap [30]. It has also been known that more surface oxygen vacancies are available upon increasing the surface-to-volume ratio for the nanoparticles. Although it seems that the formation of the e/h pairs and lowering of the bandgap are more impressive for cobalt, a synergistic effect was observed when Co-MSN(75) was doped with Zn^{2+}. **Fig. 7** illustrates the effect of Zn^{2+} content on the discoloration of basic red 5. It can be seen that increasing the Zn^{2+}/Co^{2+} *wt.%* from 1 to 7%, leads to an increase in discoloration efficiency.

The radicals in the photocatalytic reaction are responsible for degradation. The higher number of such radicals leads to a higher rate of the catalytic degradation process. In an equilibrium process, the kinetic behavior of can be explained by the Langmuir–Hinshelwood model [31]:

$$\ln(C_0/C_t) + k'(C_0 - Ct) = k'Kt = kapp\ t$$

where C is the concentration of the dye, t is time, k' is the specific reaction rate constant, K is the equilibrium constant of the reactant, C_0 is the initial concentration, C is the final concentration, and $kapp$ is the first-order rate constant. By drawing the graph of $\ln(C_0/C_t)$ versus time, $kapp$ can be obtained. The results obtained in the kinetic study of degradation dye by the metal incorporated MSN are shown in Fig. 7. By drawing the graph of $\ln(C_0/C_t)$ versus time, $kapp$ can be obtained. From the slopes of the obtained Hinshelwood plots, the apparent first-order rate constants of 0.0178,0.0225,0.0265, and 0.0362 min^{-1} for the Metal/MSNs correspond to Co-Zn(1)-MSN(75),Co-Zn(3)-MSN(75),Co-Zn(5)-MSN(75),Co-Zn(7)-MSN(75), respectively. This increase in kapp value can be attributed to the addition of Zn^{2+}.

To propose a mechanistic pathway for the title reaction, a kinetic study of the photo-degradation of basic red 5 was performed by using the Langmuir–Hinshelwood kinetics model. The reaction followed a pseudo-first-order kinetic with the apparent rate constant being calculated as $\ln C/C_0 = k_{app}t$, where C_0 is the initial

concentration and *C* is the residual concentration of the basic red 5 at the exposure time *t*, measured at room temperature in pH=7. The value of *k* for the optimized reaction catalyzed by the Co-Zn(7)-MSN(75) within the initial 45 minutes was found to be 0.0362 min^{-1} (**Fig. 8**).

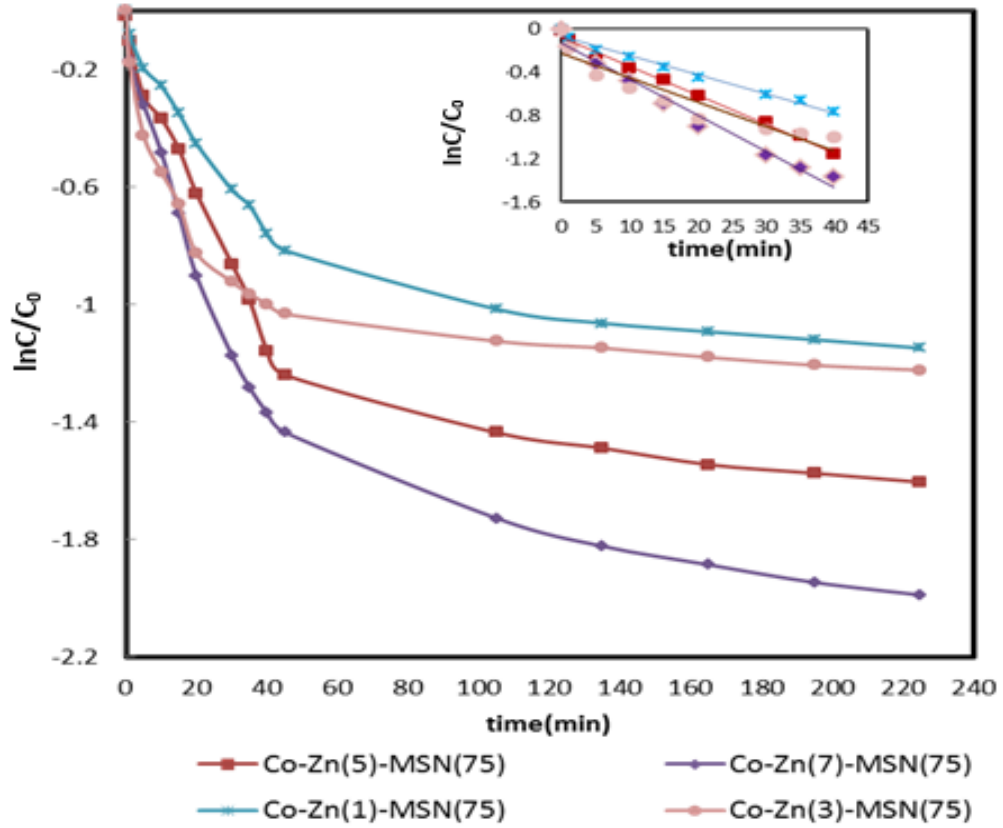

Fig. 7 Effect of the Zn^{2+} content on the efficiency of Co-MSN(75) (0.025 mg) in discoloration of basic red 5 under UV irradiation (4×8 W lamps) at pH=7 and 298 K. Inset of the figure was used for the calculation of k_{app} values.

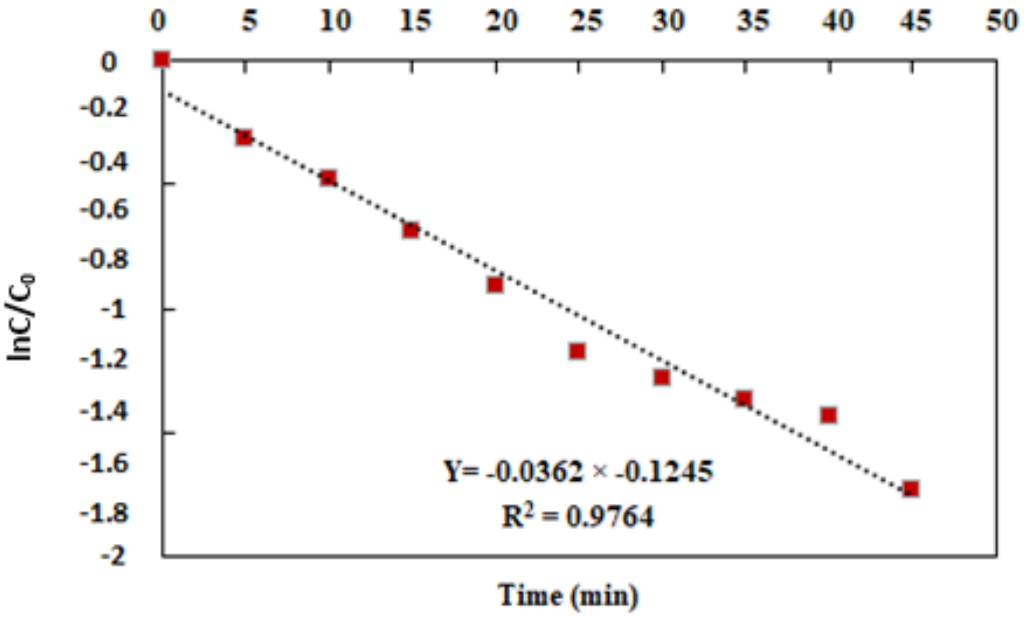

Fig. 8 Pseudo-first order k_{app} constant for the discoloration reaction of basic red 5 catalyzed by Co-Zn(7)-MSN(75) under the best conditions.

With the Co-Zn(7)-MSN(75) as the most efficient catalyst, the effect of the presence and concentration of an oxidant was also investigated. Hydrogen peroxide was selected as a cheap and affordable oxidant, and the trend of discoloration was studied at the maximum absorbance wavelength of basic red 5 (520 nm) in the range of 0.1-0.5 M H_2O_2 with and without UV irradiation. The results are presented in **Fig. 9** and show that the best result was obtained when a combination of Co-Zn(7)-MSN(75), 0.5 M H_2O_2, and 32 W UV irradiation was used. An increase in the H_2O_2 concentration from 0.1 mM to 0.5 mM resulted in an increase in the discoloration under UV radiation from 65 to 82%, respectively. Higher amounts of the oxidant, however, resulted in a decrease in dye removal. It is well known that hydrogen peroxide acts by producing hydroxyl radicals to accelerate the photocatalytic processes [4]. Hydroxyl radicals are generated by direct photolysis of hydrogen peroxide [32, 33], or by its reaction with the superoxide radicals [34-36]. It has been shown that the efficiency of the catalyst depends on the initial concentration of H_2O_2 [37]. Hydrogen peroxide plays a drastic role in the photodegradation of organic pollutants. The degradation efficiency of the photocatalyst as a function of hydrogen peroxide concentration always has to be studied as Amiri and Nezamzadeh-Ejhieh [36] and many other researchers did. Generally, more hydroxyl radicals are available when photolysis is performed in the presence of H_2O_2 under UV irradiation. Fine adjustment of the H_2O_2 concentration, however, is necessary because high concentrations of the hydrogen peroxide may result in the reaction of excess H_2O_2 with hydroxyl radicals. Determination of the optimum concentration of hydrogen peroxide has been the subject of many studies on photo-degradation of organic compounds [35, 36, 38, 39]. Most of them have shown that the effect of H_2O_2 is related to the pH of the solution [38].

The effect of the pH was also studied and the best result was obtained at pH 9 (**Fig. 10**). The correlation between the pH and efficiency of a photocatalyst is hard to explain, because there are many factors involved, including the acid-base nature of the photocatalyst, which can be explained by zero-point charge (ZPPC), and the pK_a value of the pollutant. The pKa of basic red 5 is 6.9, which lies near the first pKa of carbonic acid of 6.35. Since the pKa of basic red 5 is near neutral pH, it can be used as a carbon dioxide sensor in biological systems. Basic red 5 is in hydrochloride form in an acidic medium, and acts as a pH indicator, changing from red to yellow between pH 6.8 and 8.0. The pH zpc of the Co-Zn(7)-MSN(75) was estimated to be about 7.0, and it is anticipated that at acidic pH (lower than the pHzpc), the surface charge of the photocatalyst becomes positive due to the presence of surface hydroxyl groups, while it is negative at elevated pH [39]. Hence, in an acidic medium, the protonated basic red 5 molecules are prevented to reach the photocatalyst surface, where the photo-generated hydroxyl radicals are ready to do their duty. From **Fig. 10** it is also deducible that although the discoloration of the basic red 5 is more favorable at high pH values, convincing results can also be achieved at neutral pH when enough time is given to the system.

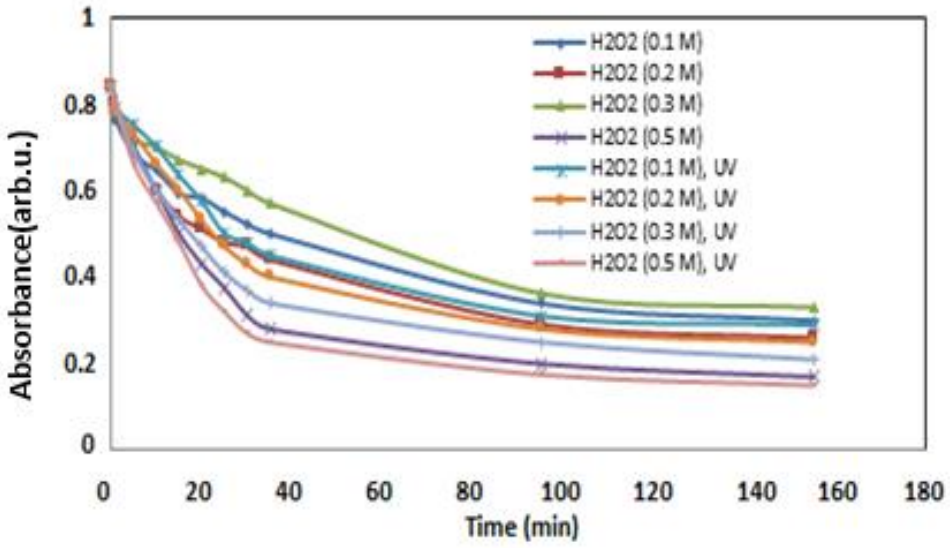

Fig. 9. Trend of basic red 5 (0.08 mM) discoloration by Co-Zn(7)-MSN(75) in the presence of H_2O_2 (0.1-0.5 M) with and without UV irradiation (4×8 W lamps) at 298 K and pH=7.

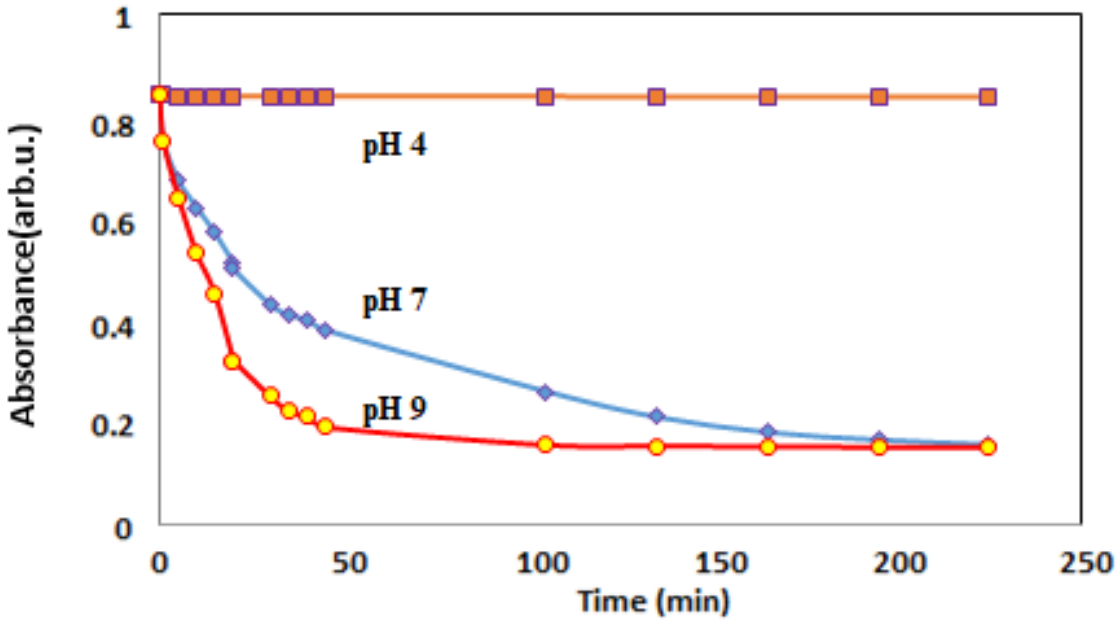

Fig. 10. Effect of pH on the discoloration of basic red 5 (0.08 mM) in the presence of Co-Zn(7)-MSN(75) and H_2O_2 (0.5 M) under irradiation of 4×8 W UV lamps; 298 K; within 225 min.

In many advanced oxidation processes (AOPs), hydroxyl radicals with an oxidation potential of 2.80 V, are responsible for the oxidation of a broad range of organic compounds [42, 43].

At high pH, H_2O_2 deprotonates to form an H_2O_2/HO_2^- equilibrium. HO_2^- reacts with H_2O_2 according to the following equation, to form O_2 and H_2O, instead of producing hydroxyl radicals under UV irradiation. Therefore, the instantaneous concentration of $OH^{\bullet}$ is lower than expected:

$$HO^-_2 + H_2O_2 \rightarrow H_2O + O_2 + OH^- \quad (2)$$

The $OH^{\bullet}$ radicals react with HO_2^- approximately 100 times faster than H_2O_2. At high pH, H_2O_2 becomes highly unstable and undergoes self-decomposition [42, 43]. The self-decomposition will rapidly break down the H_2O_2 molecules into water and oxygen as follows:

$$2H_2O_2 \rightarrow 2H_2O + O_2 \quad (3)$$

However, the better performance of the catalyst at high pH can be related to its structure. Generally, the surface of silica materials is covered by Si-OH groups. These –OH functional groups can be used, for example, in surface modification reactions. At high pH, the basic red 5 is present as a free base rather than its hydrochloride form, and this brings the molecule to the positively charged surface of the catalyst, where it can react with the oxidant.

Although according to **Fig. 10,** a faster discoloration process was observed at alkali pH, this is not suitable for wastewater treatment from technical and environmental points of view. However, from **Fig. 10** one can conclude that at neutral pH, a similar result can be obtained after 225 min with a milder rate.

The effect of the catalyst dosage was also studied. By increasing the Co-Zn(7)-MSN(75) loading from 0.010 to 0.035 mg, it was found that the optimum amount of the catalyst was 0.025 mg per mL of the dye solution. From **Fig. 11**, it is obvious that higher amounts of the catalyst did not improve the dye discoloration meaningfully, and to some extent, the efficiency of the photocatalyst was reduced. This can be justified because, at high photocatalyst dosages, aggregation of the nanoparticles and increasing the scattering effects may decrease the photon harvesting by the active sites, as discussed previously [41].

Finally, the efficiency of the modified MSNs was compared under the optimized conditions, and the results are presented in **Fig. 12**. It is clear that Co-Zn(7)-MSN(75) can be considered as a promising catalyst for discoloration of basic red 5 in the presence of 0.5 M H_2O_2 under irradiation of 4×8 W UV lamps.

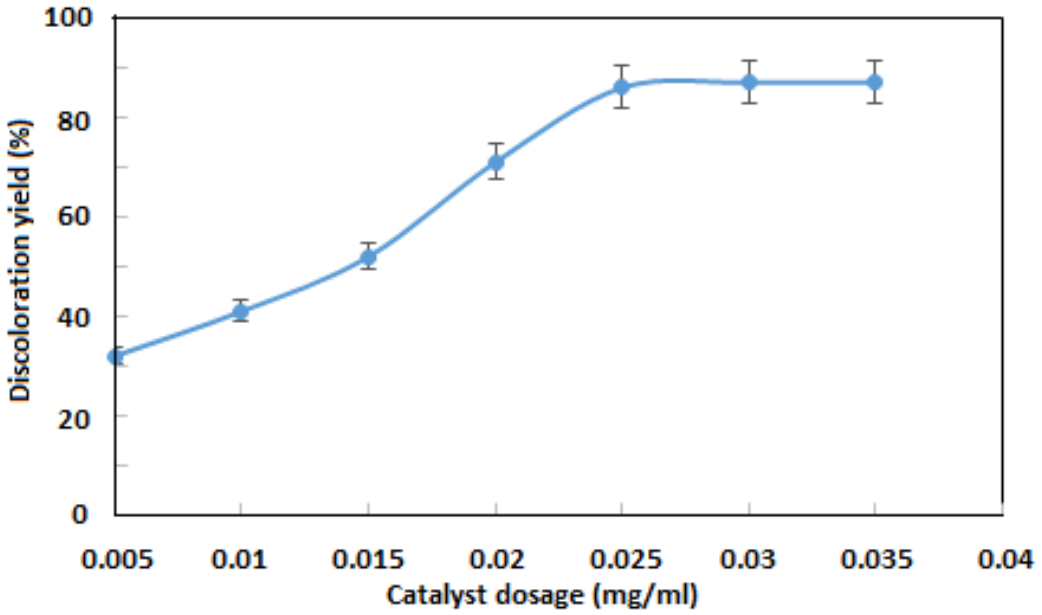

Fig. 11 Effect of the Co-Zn(7)-MSN(75) dosage on the discoloration yield of basic red 5 (0.08 mM) under the optimized conditions (0.5 M H_2O_2; irradiation of 4×8 W UV lamps; pH=7; 298 K; within 3.75 h)

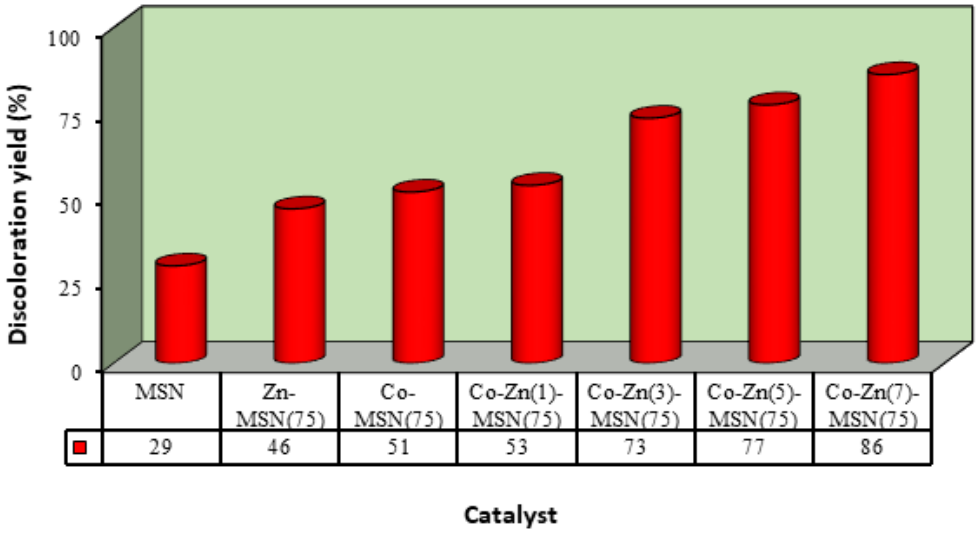

Fig. 12 A comparison of the MSN and its metal-modified forms in discoloration of basic red 5 (0.08 mM) under the optimized conditions including 0.5 M H_2O_2; irradiation of 4×8 W UV lamps; pH 7; 298 K; within 3.75 h

To visualize the changes in the UV-Vis absorbance of basic red 5 solutions upon treatment with the Co-Zn(7)-MSN(75) as the most effective photocatalyst, the trend of discoloration under the optimized conditions including 0.5 M H_2O_2 and irradiation of 4×8 W UV lamps within 3.75 h is depicted in **Fig. 13**.

In analogy with the published literature [4], it can be concluded that the following mechanistic pathway may be responsible for the discoloration of basic red 5.

1. Absorption of efficient photons by M^{2+} (M= Zn, Co);

$M^{2+} + h\upsilon \rightarrow e_{cb}^{-} + h_{vb}^{+}$

2. Oxygen sorption (first step of oxygen reduction);

$O_2 + e{-}CB \rightarrow O_2\bullet^{-}$

3. Neutralization of OH^{-} groups by photoholes which produces OH◦ radicals;

$H_2O \Leftrightarrow H^{+} + OH^{-} + h^{+}_{vb} \rightarrow H+ + OH\bullet$

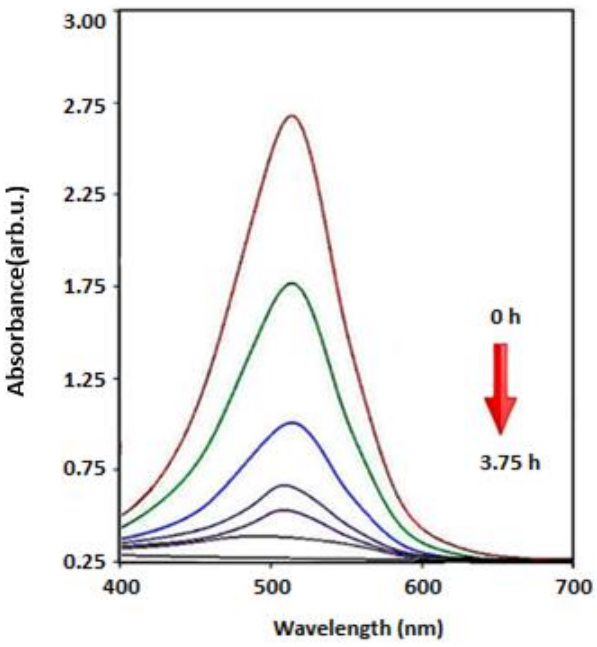

Fig. 13 Changes in the UV-Vis absorbance of basic red 5 (0.08 mM) in presence of Co-Zn(7)-MSN(75) (0.025 mg) under the optimized conditions including 0.5 M H_2O_2; irradiation of 4×8 W UV lamps; pH 7; 298 K; within 3.75 h

4. Neutralization of $O_2^{\circ -}$ by protons

$O_2^{\circ -} + H^+ \rightarrow HO_2^{\circ}$

5. Transient hydrogen peroxide formation and dismutation of oxygen;

$2HO_2^{\circ -} \rightarrow H_2O_2 + O_2$

6. Decomposition of H_2O_2 and second reduction of oxygen;

$H_2O_2 + e^- \rightarrow OH^{\circ} + OH^-$

7. Oxidation of the organic reactant via successive attacks by OH• radicals;

$R + OH^{\circ} \rightarrow R\bullet + H_2O$

8. Direct oxidation by reaction with holes;

Basic red 5 + h^+ → Basic red $5^{+\circ}$ → degradation products

Where e_{cb}^- and h_{vb}^+ refer to the electron in the conductive band and the hole in the valence band of the photo-catalyst, respectively. The role of Zn^{2+} may be justified by its role in the decrease of the bandgap.

A schematic of the photo discoloration of basic red five may be presented as **Scheme 1**.

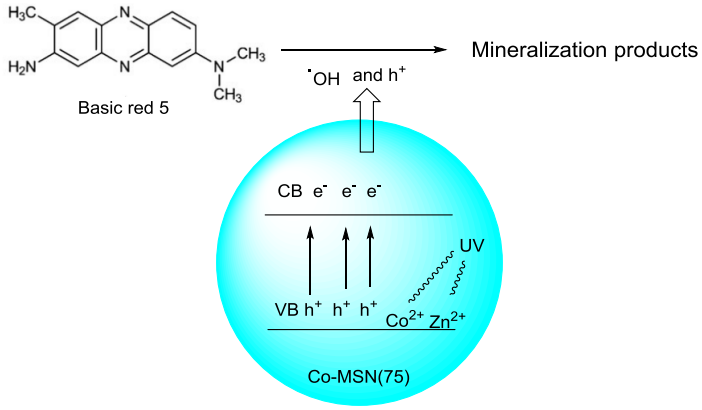

Scheme 1. Schematic discoloration of basic red 5 by Co-Zn(7)-MSN(75) photocatalyst

According to the above mechanism, UV irradiation produces a hole in the valence band of the photo-catalyst, which can oxidize a water molecule to hydroxyl radicals. These radicals can produce further hydroxyl radicals from H_2O_2. Hydroxyl radicals are generally aggressive species that can mineralize most of the organic molecules, including dyes.

It is well known that if a radical pathway is involved, the addition of a radical scavenger would interrupt the reaction. When we tested 2-propanol, the discoloration reaction was stopped, which is an indication of involving a radical mechanistic pathway. Therefore, it can be concluded that the cobalt-mediated generation of hydroxyl radicals is responsible for this type of discoloration reaction.

To compare our results with the reported cobalt-mediated methods for discoloration of basic red 5, a literature survey was undertaken and the results are summarized in **Table 2**. It can be seen that the Co-Zn(7)-MSN(75) photo-catalyzed discoloration exhibits unique advantages such as low catalyst dosage, neutral pH, ease of work-up, and above all, high efficiency.

Recyclability of the catalyst

To study the influence of the environmental matrix on the photocatalytic activity of Co-Zn(7)-MSN(75), discoloration of basic red 5 was conducted under the optimized conditions with the solutions being prepared with Tehran's Jajrood river water instead of double-distilled water. The river water was first filtered with a 0.47 µm filter and used without further purification. Up to 85% of the basic red 5 was removed according to the UV-Vis measurements at 520 nm.

To determine the reusability of the catalyst, its recovery and reuse were checked for six successive runs. The dye removal percentages obtained were 86, 84, 84, 80, 76, and 71%, which can introduce the Co-Zn(7)-MSN(75)

as a promising photocatalyst for discoloration of basic red 5.

Finally, to gain a clearer insight into the mechanism of the reaction, the effect of the radical scavenger was studied. It is well known that scavenging agents can be used to give a clue on the mechanistic pathway [49-51]. These include chloride, as the hole scavenger, HCO_3^- as the hydroxyl radical scavenger, and ascorbic acid as the superoxide scavenger. It was found that the following trend prevails: holes>hydroxyl radicals>superoxide ions. This is in agreement with our assumption reflected in the proposed mechanistic pathway. **Fig. 14** presents the results of six successive runs

Table 2. A comparison of the cobalt-mediated methods for the photocatalytic discoloration of basic red 5.

Entry	Photocatalyst	Synthesis Method	Irradiation Source	Dye conc.	Catalyst amount	Time (min)	T (°C)	pH	Efficiency (%)	Ref.
1	Co-Zn(7)-MSN(75)	Sol-Gel	32 W	0.08 mM	0.025 mg	225	25	7	86	This work
2	$Co_4[Fe(CN)_6]$	Chemical Precipitation	Tungsten lamp (200 W)	5.8×10^{-5} M	175 mg	120	-	-	68	[44]
3	Co_2SnO_4	-	Sunlight	10 mgL^{-1}	0.5 gL^{-1}	240	25	5	85	[45]
4	GNs/Co-Mn	Chenical reduction	Sunlight	5 mgL^{-1}	20 mg	30	25	7	94	[46]
5	Cobalt(II) hexacyanoferrate	Hydrothermal	UV, 50 mW cm^{-2}	5.8×10^{-5} M	150 mg	120	25	5	80	[47]
6	$LaCoO_3$	Surface ion adsorption	UV, 30 W	10 mgL^{-1}	200 mg	100	25	7	90	[48]

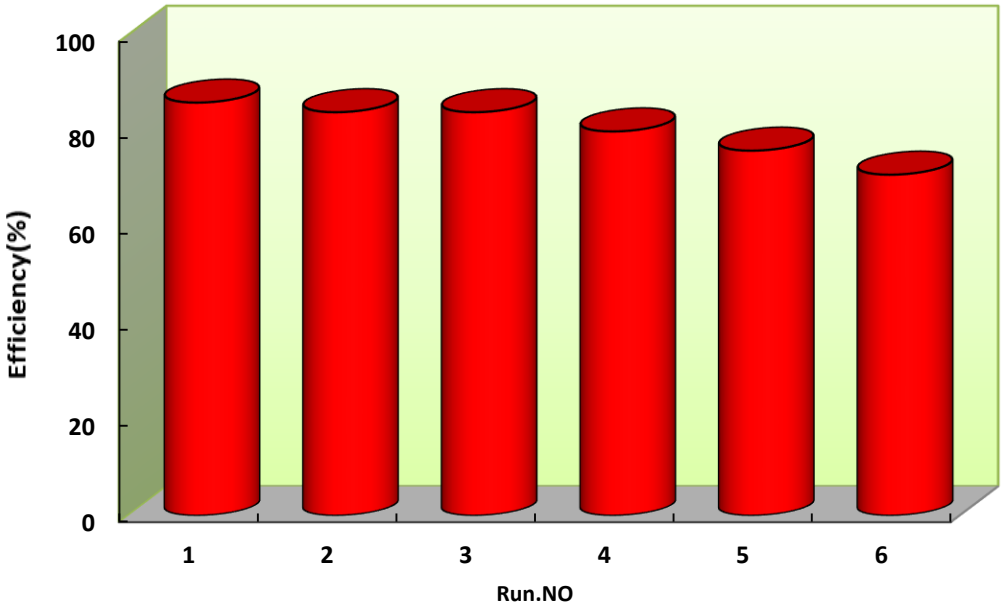

Fig14. Recyclability of the CoZn(7)-MSN(75) during six runs discoloration of basic red 5 (0.08 mM) under the optimized conditions including 0.5 M H_2O_2; irradiation of 4×8 W UV lamps; pH 7; 298 K; within 3.75 h

4. Conclusions

To be concluded, synthesis and co-modification of the mesoporous silica nanoparticles were easily achieved by the hydrothermal synthesis method. The modified mesoporous silica nanoparticles including Co-MSN(75) and Zn-MSN(75) (with Si/Co and Si/Zn molar ratio of 75), and Co-Zn(X)-MSN(75) with different Zn^{2+} contents of 1-7 *wt*.% relative to Co^{2+}, were fully characterized. The most obvious aspects of this type of modification were reflected in the physicochemical properties of the modified MSNs, including an increase of the d_{100}-spacing as a result of M^{2+} inclusion, a decrease in the specific surface areas, and partial pore blockage. At the expense of these structural changes, however, the photocatalytic activity of the modified MSNs increased significantly. The photocatalytic activity of the obtained catalysts was studied for the discoloration of basic red 5 as a representative dye. Effect of various parameters such as pH, dye and catalyst concentration, amount of oxidant, and presence/absence of UV irradiation was investigated. UV irradiation considerably improved the discoloration efficiency and the best results were obtained by using an array of 4×8 W (254 nm) UV lamps. Further improvement was achieved when hydrogen peroxide was used as an oxidant. Although more hydroxyl radicals are available when photolysis is performed in presence of hydrogen peroxide, it was observed that high concentrations of hydrogen peroxide had an adverse effect due to the reaction of excess H_2O_2 with hydroxyl radicals. A study of the pH effect showed that at higher pH values, the discoloration was performed more readily. From a green chemistry point of view, however, pH 7 was used as the working pH. Under the optimized conditions including pH=7, 0.08 mM of dye concentration at 298 K, and irradiation of 4×8 W (254 nm) UV lamps, up to 86% of basic red 5 was discolored after 225 min in presence of 0.025 mg of Co-Zn(7)-MSN(75).

References

[1] E. Borenfreund, J.A. Puerner, T Toxicol. Lett. 24 (1985) 119-124.

[2] H. Zollinger, Color Chemistry: syntheses, properties, and applications of organic dyes and pigments, John Wiley & Sons, New York, 2003.

[3] M. Iram, C. Guo, Y. Guan, A. Ishfaq, H. Liu, J. Hazard. Mater. 181 (2010) 1039-1050.

[4] M.M. Alnuaimi, M. Rauf, S.S. Ashraf, Dyes Pigm. 76 (2008) 332-337.

[5] F.M. Mpatani, A.A. Aryee, A.N. Kani, Q. Guo, E. Dovi, L. Qu, Z. Li, R. Han, Chemosphere, (2020) 127439.

[6] Y. Rong, Y. Huang, P. Jin, C. Yang, Z. Zhong, C. Dong, W. Liang, J. Water Process. Eng. 37 (2020) 101345.

[7] Y. Yao, G. Teng, Y. Yang, B. Ren, L. Cui, Sep. Purif. Technol. 227 (2019) 115684.

[8] J. Li, C. Shi, H. Zhang, X. Zhang, Y. Wei, K. Jiang, B. Zhang, Chemosphere, 218 (2019) 984-991.

[9] T. Yanagisawa, T. Shimizu, K. Kuroda, C. Kato, Bull. Chem. Soc. Jpn. 63 (1990) 988-992.

[10] C. Kresge, M. Leonowicz, W.J. Roth, J. Vartuli, J. Beck, Nature, 359 (1992) 710-712.

[11] A. Mourhly, M. Kacimi, M. Halim, S. Arsalane, Int. J. Hydrogen Energy 45 (2020) 11449-11459.

[12] P.T. Sharma, S. Choudhury, V. Chowdary, Mobile Sensors Deployment Methods: A Review, Intelligent Communication, Control and Devices, Springer 2020, pp. 883-893.

[13] E. Bagheri, L. Ansari, E. Sameiyan, K. Abnous, S.M. Taghdisi, M. Ramezani, M. Alibolandi, Biosens. Bioelectron. 153 (2020) 112054.

[14] W. Lei, C. Sun, T. Jiang, Y. Gao, Y. Yang, Q. Zhao, S. Wang, Mater. Sci. Eng. C 105 (2019) 110103.

[15] Y. Shen, M. Li, T. Liu, J. Liu, Y. Xie, J. Zhang, S. Xu, H. Liu, Int. J. Nanomed. 14 (2019) 4029.

[16] D.F. Mohamad, N.S. Osman, M.K.H.M. Nazri, A.A. Mazlan, M.F. Hanafi, Y.A.M. Esa, M.I.I.M. Rafi, M.N. Zailani, N.N. Rahman, A.H. Abd Rahman, Mater. Today Proc. 19 (2019) 1119-1125.

[17] M.R. Sazegar, A. Dadvand, A. Mahmoudi, RSC Adv. 7 (2017) 27506-27514.

[18] H.C. Tayefe, M.R. Sazegar, A. Mahmoudi, K. Jadidi, Silicon, (2020) 1-10.

[19] J. Zhu, T. Wang, X. Xu, P. Xiao, J. Li, Appl. Catal. B Environ. 130 (2013) 197-217.

[20] V.A. Valles, Y. Sa-ngasaeng, M.L. Martínez, S. Jongpatiwut, A.R. Beltramone, Fuel, 240 (2019) 138-152.

[21] N.G. Hajiagha, A. Mahmoudi, M.R. Sazegar, M.M. Pouramini, Microporous Mesoporous Mater. 274 (2019) 43-53.

[22] H. Choopan Tayefe, M.R. Sazegar, A. Mahmoudi, K. Jadidi, J. Nanostruct. 9 (2019) 712-722.

[23] M. Rezaei, A. Nezamzadeh-Ejhieh, Int. J. Hydrogen Energ. 45 (2020): 24749-24764.

[24] N. Raeisi-Kheirabadi, A. Nezamzadeh-Ejhieh, Int. J. Hydrogen Energ. 45 (2020): 33381-33395.

[25] F. Mahfoozi, A. Mahmoudi, M.R. Sazegar, K. Nazari, J. Sol-Gel Science &Technology.100 (2021) 170-182.

[26] S. Kumari, B.B. Dhar, C. Panda, A. Meena, S. Sen Gupta, ACS Appl. Mater. 6 (2014) 13866-13873.

[27] N. Jusoh, A. Jalil, S. Triwahyono, H. Setiabudi, N. Sapawe, M. Satar, A. Karim, N. Kamarudin, R. Jusoh, N. Jaafar, Appl. Catal. A 468 (2013) 276-287.

[28] M. Sazegar, A. Jalil, S. Triwahyono, R. Mukti, M. Aziz, M. Aziz, H. Setiabudi, N. Kamarudin, Chem. Eng. J. 240 (2014) 352-361.

[29] N.A. Neto, B. Dias, R. Tranquilin, E. Longo, M. Li, M. Bomio, F. Motta, J Alloys Compd. 823 (2020) 153617.

[30] S. Singh , R. Sharma, B. Raj Mehta, Appl. Surf. Sci. 411 (2017) 321–330

[31] a) Chem. Phys. Lett. 759 (2020) 137873. , b)Iran. J. Catal. 11 (2021) 247-259, c)Iran. J. Catal.11, 2021, 1-11, d) Desal. Water Treat. 197 (2020) 200-212

[32] V. Binas, D. Venieri, D. Kotzias, G. Kiriakidis, J. Materiomics 3 (2017) 3-16.

[33] D.F. Ollis, E. Pelizzetti, N. Serpone, Environ. Sci. Technol. 25 (1991) 1522-1529.

[34] C.S. Turchi, D.F. Ollis, J. Catal. 122 (1990) 178-192.

[35] I. Poulios, E. Micropoulou, R. Panou, E. Kostopoulou, Appl. Catal. B Environ. 41 (2003) 345-355.

[36] M. Amiri, A. Nezamzadeh-Ejhieh, Mat. Sci. Semicond. Proc. 31 (2015): 501-508.

[37] M. Czaplicka, J. Hazard. Mater. 134 (2006) 45-59.

[38] D.D. Dionysiou, M.T. Suidan, I. Baudin, J.-M. Laîné, Appl. Catal. B Environ. 50 (2004) 259-269.

[39] A. Pourtaheri, A. Nezamzadeh-Ejhieh, Spectrochim Acta A: Mol. Biomol. Spect. 137 (2015): 338-344.

[40] L. Furatian, M. Mohseni, J. Photochem. Photobiol. A: Chem. 356 (2018) 364-369.

[41] F. Soori, A. Nezamzadeh-Ejhieh, J. Mol. Liq. 255 (2018): 250-256.

[42] T. Oppenländer, Photochemical purification of water and air: advanced oxidation processes (AOPs)-principles, reaction mechanisms, reactor concepts, John Wiley & Sons, New York, 2007.

[43] C. Chan, S. Tao, R. Dawson, P. Wong, Environ. Pollut. 131 (2004) 45-54.

[44] A. Eyasu, O. Yadav, R. Bachheti, Int. J. Chem. Tech. Res. 5 (2013) 1452–1461.

[45] H. Bouchaaba , B. Bellal, R. Maachi, M. Trari , N. Nasrallah , A. Mellah, J. Taiwan Instit. Chem. Eng. 58 (2016): 310-317.

[46] K. Saeed, I. Khan, Turkish J. Chem. 41 (2017) 391-398.

[47] O. Sharma, M. K. Sharma, Int. J. Chem. Tech. Res. 5 (2013) 1615-1622.

[48] S. Fu, H. Niu, Z. Tao, J. Song, C. Mao, S. Zhang, C. Chen, D. Wang, J. Alloys Compd. 576 (2013) 5-12.

[49] S. Ghattavi, A. Nezamzadeh-Ejhieh, J. Mol. Liq. 322 (2021): 114563.

[50] S. Ghattavi, A. Nezamzadeh-Ejhieh, Desalin. Water Treat. 166 (2019): 92-104.

[51] S. Ghattavi, A. Nezamzadeh-Ejhieh, Int. J. Hydrog. Energy 45 (2020): 24636-24656.